The Efficiency of Elemental Geochemistry and Weathering Indices as Tracers in Aeolian Sediment Provenance Fingerprinting

Kazem Nosrati (k_nosrati@sbu.ac.ir)
Shahid Beheshti University
Hanieh Moradian
Shahid Beheshti University
Mojtaba Dolatkordestani
Shahid Beheshti University
Adrian L. Collins
Rothamsted Research

Research Article

Keywords: Modified MixSIR, sand dune tracing, weathering, mulch, wind break

Posted Date: February 26th, 2021

DOI: https://doi.org/10.21203/rs.3.rs-244787/v1

Version of Record: A version of this preprint was published at CATENA on March 1st, 2022. See the published version at https://doi.org/10.1016/j.catena.2021.105932.

Abstract

Eight geochemical elements (Al, Ca, Fe, K, Na, Mg, Si, Ti) and 17 associated weathering indices were measured in 34 aeolian source samples and 10 sand dune target sediment samples in three absolute particulate size fractions. For each fraction, three final composite fingerprints (i.e., geochemical elements only, weathering indices only and a combination of the two) for discerning and ascribing the aeolian sediment sources were selected. The Modified MixSIR Bayesian un-mixing model was used to apportion aeolian source contributions using the final composite fingerprints. Regardless of the composite fingerprint used, all results across the different size fractions suggested that the south-eastern alluvial fan is the dominant (average contribution 50.6%, SD 19.0%) source of the sand dune samples, with the western alluvial fan being the second most important (average contribution 38.4%, SD 20.4%) source. Comparisons of the posterior distributions for the predicted source proportions generated using the nine composite fingerprints (three kinds of composite fingerprints*three particle size fractions) showed that the composite fingerprints combining the geochemical elements and weathering indices generated the most powerful source material discrimination. Our results demonstrate the use of weathering indices alongside more conventional elemental geochemistry tracers for investigations into sand dune sediment provenance.

1. Introduction

Wind erosion has three stages comprising abrasion, deflation, and accumulation [1]. Prevailing winds cause the redistribution, accumulation and migration of sand in many regions of the world. The principal controlling factors for sand dune formation include wind direction and velocity, the available supply of sand in source areas subject to wind erosion, source area surface roughness, aggregate stability, presence of crusting, soil texture and moisture, vegetation cover and the presence of residues [2–4]. Effective wind erosion mobilises erodible soil particles, which can be deposited subsequently on agricultural land, roads and railways, and in settlements. Given these on-site and off-site consequences of wind erosion [5,6], there is a need to determine the key sources of aeolian sediment in order to target and select robust strategies for stabilising the source areas.

Most areas of arid land in central Iran are under threat of aeolian deposits (landforms) resulting from wind erosion. Due to strong prevailing winds and the lack of moisture and vegetation cover, both fine and coarse soil particles are redistributed to depositional zones where sand dunes form. Sand dunes have been estimated to cover 12 million ha in Iran, with approximately 50% being classified as active or semiactive [7]. Available solutions for controlling the threat of sand dune formation and migration include stabilizing sand dune areas with mixed petroleum and tar mulching, removing sand dunes, and either biological or mechanical windbreaks [2,8,9]. But, despite application of these interventions, the disbenefits arising from sand dune formation and migration continue to be severe in Iran. Here, for instance, some studies have reported that petroleum and tar mulching whilst an effective method for sand dune stabilization and reducing storm dust [10] can result in environmental pollution resulting from heavy

metals. The alternative approach to management is to focus on identifying the key sources of aeolian sediment to target interventions for decreasing the supply of sand generating off-site aeolian sediment deposits (i.e., sand dunes).

Traditional techniques for quantifying aeolian sediment provenance were based on the shape and texture of dune sands, and an abrasion coefficient (i.e., sphericity of particles). These methods estimate the distance of particle transport and on that basis estimate the sources of dune sand. An alternative approach is to use source fingerprinting which is founded on the direct comparison of the properties, or composite fingerprints, of dune deposits and potential source areas. Early studies based on aeolian sediment properties used light and/or heavy mineral compositions as well as minor element geochemistry [11–14]. These studies did not, however, use an un-mixing model to estimate the contribution of each source on the basis of the fingerprint properties analysed. More recently, as global uptake of the fingerprinting approach has continued to expand, especially in fluvial environments [15–17], applications to aeolian sediment and storm sand tracing have also started to emerge [18–20]. Here, since applications to aeolian systems are rudimentary, in comparison with those in fluvial environments, there remains a need to explore the most reliable and cost-benefit tracers to discriminate and apportion sources. In this context, weathering indices have proved to be useful for investigating fluvial sediment sources [21–23], but their applicability to the aeolian sediment problem warrants further research.

Globally, weathering and erosion generate quartz and silicate dune sediments from quartz-rich rocks but, locally, sand deposits can consist of grains weathered from carbonate or by near-surface chemical and physical processes [24]. Dune sands originating from the weathering of bedrock appear to be limited whereas contributions from eroding fluvial sediment deposits are more common [25]. Collectively, this means that physical, chemical, and mechanical weathering can all play a role in the earth surfrace processes generating dune sediments [26,27]. Accordingly, weathering indices have the potential to provide useful tracers for aeolian source discrimination and apportionment since they reflect the susceptibility of potential source areas to wind erosion arising from interactions between climate, geology, pedology, tectonic processes, relief, land cover and human activity [27,28]. The main objective of this study, accordingly, was to apportion aeolian sediment source contributions to aeolian target sediment (i.e., sand dune deposits) samples comprising different particle size fractions in a case study located within central Iran, using geochemical properties and weathering indices as tracers and the Bayesian un-mixing model MixSIR.

2. Materials And Methods

2.1. Study area

The Hoseinabad Mish Mast region (340 km^2) is located in the central part of Iran in boundary Qom and Isfahan Provinces between 51° 02' 29" to 51° 15' 29" E longitude and 34° 18' 06" to 34 34' 44" N latitude. The topography of the study area includes plain, piedmont and hills. Maximum elevations are up to 1039

m whereas the minimum elevation is 805 m above sea level. Eastern parts of the study region comprise hilly terrain (maximum slope of 40%). Much of the study area is, however, flat. Land use is dominated by rangelands and cultivated land. Based on the 1:100,000 scale lithology map of Qom (Fig. 1), the main lithology comprises: upper red formation (marl with intercalations of conglomerate); marl with intercalations of sandstone, gypsum, and siltstone; association of marl, shale and greyish green caverneous sandstone with gypsiferous marl; association of greyish red to brown sandstone, conglomerate and marl; conglomerate with calcareous pebbles; red marl, shale, siltstone, dark red gypsiferous sandstone, gypsum and dark green sandstone in some localities); lower red formation (alternation of red and dark grey silty shale, sandy marl, green marl with intercalations of sandstone, gypsum and salt); the Qom formation (marl, limestone, sandstone, shale, gypsum and volcanic rocks in some localities), and a Quaternary unit (young alluvial terraces; old alluvial terraces; recent river deposits; scree; sand dunes; salty mud flat). Based on data (1986–2015) collected by the Qom synoptic station, the mean annual rainfall is ~ 144 mm (coefficient of variation 43%). Long term (1986–2015) mean monthly minimum / maximum temperatures are 4.6°C and 31.4°C, respectively. According to the Köppen climate classification scheme, the climate of the study area is dry desert. The dominant winds in the study area are western and north-western (Fig. 1).

The case study area is recognised as being fragile and susceptible to wind erosion (Fig. 2a). The village of Hoseinabad Mish Mast has been surrounded by mobile sand dunes (Fig. 2b). The Sarajeh gas installation (one of the most important gas installations in the Qom Province; Fig. 2c) and associated roads (Fig. 2d) as well as the main railway (Fig. 2e) in this region are all threatened by mobile sand dunes. In total, 271 km^2 of this region is identified as being at risk from the aeolian sediment problem. In response, interventions comprising petroleum and tar mulching (Fig. 2f) and windbreaks (Fig. 2e&g) have been used to control the threat of the aeolian sediment hazard. These methods do not, however, deliver sustained efficiency meaning that the dunes continue to migrate (Fig. 2e&h). Consequently, there is an urgent need to quantify the sources of the aeolian sediments instead of relying on methods to stabilise sand dunes.

2.2. Field sampling, geochemical tracer measurements, and calculation of weathering indices

Identification of potential aeolian sediment sources: In order to prepare a map of potential aeolian sediment sources the location of aeolian sediment deposits (i.e., sand dunes) was determined (Fig. 1). Next, the wind rose for the study area based on the wind data collected at the Qom synoptic meteorological station was prepared. By merging the dominant wind directions and the mapped locations of sand dunes and considering the mountains (which act as barriers to the winds) surrounding the study area, the key potential aeolian sediment sources were determined (Fig. 1). Using Google Earth images and field surveys, three potential sources of aeolian sediment were identified: crop lands, western alluvial fans, and south-eastern alluvial fans (Fig. 1).

Aeolian sediment source sampling: based on a random-systematic sampling design, a total of 34 samples were collected from the potential aeolian sediment sources: 14 samples from crop lands, 11 samples from the western alluvial fans, and a further 9 samples from the south-eastern alluvial fans (Fig. 1). Each sample represented a composite combining five sub-samples to take account of potential micro-spatial (i.e., within ~ 100 m^2) variations in geochemical elements at each individual sampling location selected to represent the sources. The sampling depth was ~ 5 cm to represent the typical depth of wind erosion effects.

Sand dune sampling: 10 samples were collected from sand dunes based on a random-systematic approach (Fig. 1). Each sample was composited from three sub-samples that were collected from the windward, crest, and leeward sides of the sampled sand dunes.

Determining the dominant particle fractions: in order to assess the particle size distribution of the target sand dune samples for confirming the most appropriate fraction for source fingerprinting , dry-sieving was performed using 1000, 500, 425, 250, 180, 150, 125, 75, and 63 µm meshes to determine the dry mass in each fraction. Based on the cumulative frequency curves (Fig. 3) three absolute particle size fractions comprising <125 µm, 125-250 µm, and 250-425 µm, were selected as the dominant fractions.

Measurements for geochemical elements: Acid digestion was used for elemental extraction for all samples of the three fractions. 1 g of sample was weighed; 3 ml of Nitric acid and 9 ml of Hydrochloric acid added and after 24 h, all samples were heated for 2 h on a hotplate at 90 ˚C. After the digestion, the samples were filtered and diluted to a volume of 50 ml. Al, Ca, Fe, K, Na, Mg, Si, and Ti were measured in the solutions using a Varian SpectrAA-20 Plus. An element standard solution (Merck KGaA, Frankfurt, Germany) and standard curve was used to calculate the element concentrations based on the dilution factor.

Evaluation of elemental tracer content in the three particle size fractions: As the absolute particle size analysis suggested a broad size range was representative of the target sediment samples, it was informative to analyse the elemental tracers in the size fractions to confirm it was appropriate to use all fractions for determining sediment sources with the tracers in question. Here, one-way ANOVA was used to evaluate the presence of significant contrasts between the content of individual tracers in the different size fractions.

Calculation of weathering indices: 17 weathering indices (Table 1) were calculated. All elements were transformed to oxide percent and then the molecular weights of elemental oxides were calculated using molar mass. Finally, based on the formulas presented in Table 1, the different weathering indices were calculated.

Summary statistics for all geochemical elements and weathering indices are presented in Table 2.

Table 2

Tracer concentration (%) and weathering indices data for the different sand dune sources and target sand dune samples, plusthe Kruskal-Wallis H-test results for discriminating the sources using the individual tracers in the three dominant absolute particle size fractions. For tracer abbreviations see Table 1.

Tracer	Aeolian sediment sources						Kruskal-Wallis H-test		Target sand dune samples (n = 10)	
	Crop lands (n = 14)		Western alluvial fans (n = 11)		South-eastern alluvial fans (n = 9)					
	Mean	SD	Mean	SD	Mean	SD	H value	p-value	Mean	SD
< 125 µm fraction										
Al	4.49	0.22	3.94	0.66	4.17	0.38	7.5	0.02*	4.28	3.27
Ca	3.48	0.63	2.82	1.75	3.54	1.18	2.6	0.27	2.92	1.07
Fe	0.96	0.2	0.86	0.15	0.91	0.04	n.c.	n.c.	1.1	0.7
K	3.14	0.34	2.57	0.73	2.9	0.53	n.c.	n.c.	2.37	1.84
Na	0.78	0.22	0.51	0.08	0.87	1.06	12.0	0.002*	0.65	0.42
Mg	3.18	0.7	2.07	0.62	3.1	0.47	15.4	< 0.001*	2.19	1.44
Si	13.66	3.2	11.28	1.78	17.43	3.6	15.0	< 0.001*	16.5	9.49
Ti	0.15	0.01	0.14	0.01	0.15	0.01	n.c.	n.c.	0.17	0.13
CIA	36.87	3.58	40.57	11.05	35.48	5.82	1.3	0.5	40.43	29.65
MWPI	32.55	3.6	29.18	3.69	28.14	4.79	n.c.	n.c.	23.82	23.34
WIP	68.86	7.88	52.36	11.35	67.41	15.78	13.1	0.001*	52.9	41
PI	83.18	2.55	82.67	2.01	87.2	1.95	15.2	< 0.001*	86.03	80.66
CIW	44.82	4.75	50.15	16.46	43.21	9.21	1.1	0.6	47.89	33.99
PIA	29.76	5.2	37.1	17.47	28.33	7.13	2.3	0.31	36.26	21.19
RI	0.54	0.09	0.81	0.28	0.55	0.15	11.2	0.003*	0.76	0.44
SA(RR)	5.82	1.23	5.75	0.82	8.09	2.01	14.4	< 0.001*	7.4	4.74
VR	0.53	0.05	0.66	0.17	0.5	0.11	5.9	0.053	0.62	0.38
Si-Ti	0.03	0.002	0.04	0.005	0.03	0.002	n.c.	n.c.	0.04	0.03

* n.c. non-conservative; ** Critical p-value = 0.05. KW-H test, Kruskal-Wallis H-test.

Tracer	Aeolian sediment sources						Kruskal-Wallis H-test		Target sand dune samples (n = 10)	
	Crop lands (n = 14)		Western alluvial fans (n = 11)		South-eastern alluvial fans (n = 9)					
	Mean	SD	Mean	SD	Mean	SD	H value	p-value	Mean	SD
Kr	5.26	1.08	5.03	0.74	7.31	1.8	15.2	< 0.001*	6.55	4.18
ACN	0.59	0.03	0.62	0.02	0.59	0.08	n.c.	n.c.	0.64	0.51
AKN	1.47	0.18	1.67	0.2	1.52	0.4	n.c.	n.c.	1.78	1.29
ALK	70.63	5.19	73.66	5.79	71.35	14.2	3.7	0.16	68	65.44
Lc	1.76	0.31	2.05	0.36	2.33	0.64	n.c.	n.c.	2.83	1.44
Rc	0.33	0.03	0.41	0.09	0.31	0.05	n.c.	n.c.	0.43	0.26
SOC	0.92	0.04	0.8	0.13	0.85	0.07	7.6	0.02*	0.89	0.76
125–250 µm fraction										
Al	5.06	0.18	4.41	0.79	4.86	0.46	4.7	0.09	4.83	0.06
Ca	4.51	1.73	4.04	2.85	5.71	3.15	4.7	0.09	4.58	0.97
Fe	5.31	0.19	5.99	2.34	7.06	2.43	n.c.	n.c.	6.72	2.22
K	3.19	0.38	2.63	0.36	2.69	0.32	11.6	0.003*	2.65	0.19
Na	1.42	0.4	0.73	0.25	0.77	0.37	16.2	< 0.001*	0.89	0.06
Mg	3.11	0.72	2.05	0.36	3.06	0.67	16.0	< 0.001*	2.16	0.18
Si	19.33	9.05	12.38	1.03	23.56	7.21	19.5	< 0.001*	21.37	2.32
Ti	0.14	0.008	0.13	0.01	0.14	0.01	1.5	0.47	0.14	0.008
CIA	34.55	5.64	36.9	8.12	33.76	9.19	3.1	0.21	35.3	3.19
MWPI	28.56	5.59	28.64	5.7	24.85	4.83	n.c.	n.c.	21.94	1.6
WIP	82.28	11.07	61.56	11.18	73.16	11.37	13.5	0.001*	64.39	4.75
PI	81.53	4.22	76.78	3.5	83.86	4.09	11.8	0.002*	83.47	2.25
CIW	40.88	7.81	43.88	10.28	38.95	11.38	2.6	0.27	40.42	3.94

* n.c. non-conservative; ** Critical p-value = 0.05. KW-H test, Kruskal-Wallis H-test.

Tracer	Aeolian sediment sources						Kruskal-Wallis H-test		Target sand dune samples (n = 10)	
	Crop lands (n = 14)		Western alluvial fans (n = 11)		South-eastern alluvial fans (n = 9)					
	Mean	SD	Mean	SD	Mean	SD	H value	p-value	Mean	SD
PIA	26.5	5.29	28.09	8.61	26.2	9.68	n.c.	n.c.	28.51	3.83
RI	0.43	0.11	0.62	0.19	0.48	0.19	7.8	0.02*	0.58	0.07
SA(RR)	7.29	3.21	5.51	0.78	9.25	2.43	12.5	0.002*	8.49	0.95
VR	0.5	0.09	0.61	0.14	0.46	0.11	10.7	0.005*	0.54	0.05
Si-Ti	0.03	0.001	0.03	0.004	0.03	0.002	12.9	0.001*	0.03	0.001
Kr	4.82	2.08	3.39	0.65	5.54	1.57	11.8	0.003*	5.14	0.78
ACN	0.56	0.03	0.62	0.03	0.63	0.04	15.4	< 0.001*	0.63	0.01
AKN	1.33	0.19	1.65	0.2	1.81	0.36	15.4	< 0.001*	1.74	0.12
ALK	57.42	7.64	68.32	6.34	68.17	8.13	11.5	0.003*	62.14	2.89
Lc	2.32	1.12	1.97	0.39	2.67	0.82	n.c.	n.c.	2.98	0.3
Rc	0.46	0.07	0.6	0.16	0.5	0.15	8.2	0.02*	0.58	0.08
SOC	1.41	0.04	1.35	0.33	1.53	0.28	1.8	0.4	1.49	0.2
250–425 µm fraction										
Al	4.99	0.14	4.49	0.66	5.06	2.82	3.4	0.19	4.8	0.1
Ca	4.3	1.09	5.21	4.98	6.52	3.98	n.c.	n.c.	4.16	1.17
Fe	1.69	0.14	1.58	0.21	6.38	2.94	19.8	< 0.001*	5.33	0.13
K	3.01	0.47	2.24	0.51	2.54	0.43	12.2	0.002*	2.76	0.53
Na	0.12	0.03	0.07	0.02	0.06	0.03	13.1	0.001*	0.07	0.005
Mg	3.04	0.7	2.3	0.3	3.12	0.94	7.1	0.03*	2.25	0.17
Si	8.83	0.09	8.74	0.06	8.88	0.08	n.c.	n.c.	9.04	0.09
Ti	0.14	0.007	0.13	0.01	0.14	0.01	2.6	0.27	0.14	0.003
CIA	38.8	4.51	38.22	12.39	32.88	21.39	n.c.	n.c.	39.19	4.07

* n.c. non-conservative; ** Critical p-value = 0.05. KW-H test, Kruskal-Wallis H-test.

Tracer	Aeolian sediment sources						Kruskal-Wallis H-test		Target sand dune samples (n = 10)	
	Crop lands (n = 14)		Western alluvial fans (n = 11)		South-eastern alluvial fans (n = 9)					
	Mean	SD	Mean	SD	Mean	SD	H value	p-value	Mean	SD
MWPI	39.19	3.04	37	8.59	40.83	6.16	n.c.	n.c.	33.64	2.79
WIP	61.6	7.53	53.04	18.51	64.49	11.75	9.5	0.008*	54.43	7.12
PI	73.97	0.48	75.72	2.63	67.95	7.46	13.5	0.001*	69.7	0.31
CIW	46.44	6.66	44.26	12.11	37.98	14.14	n.c.	n.c.	46.5	5.56
PIA	33.71	6.09	34.58	11.6	26.48	16.19	5.2	0.07	34.37	5.3
RI	0.64	0.12	0.8	0.28	0.54	0.26	8.9	0.01*	0.68	0.18
SA(RR)	3.40	0.08	3.82	0.65	14.18	1.89	2.1	0.34	3.61	0.09
VR	0.56	0.07	0.56	0.14	0.46	0.3	n.c.	n.c.	0.63	0.08
Si-Ti	0.03	0.001	0.03	0.004	0.03	0.02	2.8	0.24	0.03	0.001
Kr	2.92	0.07	3.26	0.52	2.37	1.03	n.c.	n.c.	2.35	0.03
ACN	0.69	0.02	0.73	0.04	0.7	0.08	6.7	0.03*	0.7	0.03
AKN	2.28	031	2.81	0.51	2.7	1.22	6.7	0.03*	2.47	0.45
ALK	93.3	1.86	94.41	1.51	95.67	1.96	7.3	0.02*	95.3	0.76
Lc	1.16	0.14	1.36	0.33	1.01	0.21	n.c.	n.c.	1.4	0.16
Rc	0.33	0.05	0.42	0.11	0.49	0.25	n.c.	n.c.	0.95	0.06
SOC	1.07	1.03	0.97	0.13	1.51	0.53	14.4	< 0.001*	1.36	0.01

* n.c. non-conservative; ** Critical p-value = 0.05. KW-H test, Kruskal-Wallis H-test.

2.3. Sand dune source discrimination and apportionment

In total, 25 potential tracers comprising eight geochemical elements and 17 weathering indices were tested for discriminating and apportioning sand dune sources in the three particle size fractions based on final composite fingerprints comprising: 1) using only geochemical elements; 2) using only weathering indices, and; 3) combining the geochemical elements and weathering indices. This yielded a total of nine final composite fingerprints. In all three approaches, conservation tests were undertaken. Here, in first step, the tracer values for the target sand dune samples were compared to the range based on the tracer

values for the individual sources (i.e., the minimum average source value minus its standard deviation and the maximum source average value plus its standard deviation). Any tracer exhibiting a target aeolian sediment sample value outside of the corresponding source range was excluded from further statistical analysis. In the second step of the conservation tests, the mean tracer values for all target sand dune samples were compared to the minimum and maximum mean values for the sources. Again, violation of this conservation test was used as a basis for identifying redundant tracers. In order to be sure that tracer concentrations had not been affected by sand dune transportation and sedimentation processes, the final sets of tracers for discriminating the sand dune sources were assessed using biplots of tracer concentrations in source and target sand dune samples for all three particle size fractions. The use of biplots as an additional test of tracer conservation is now recognised as a useful step in state-of-the-art source fingerprinting decision trees [15].

For selecting three final composite fingerprints for each particle size fraction (i.e., the nine final signatures) a two step statistical procedure comprising the Kruskal-Wallis H-test (KW-H) as step one and discriminant function analysis (DFA) as step two was used in conjunction with the tracers passing the conservative tests. This confirmed the composite fingerprints for discriminating sand dune sources. DFA statistics comprised Wilks' Lambdas, partial Lambdas, F to remove, the p-levels, the tolerance and 1-tolerance values, and a full canonical analysis (eigenvalues, canonical correlation, Wilks' lambda, Chi-Square, p-level) for all functions, as well as classification and associated scatter plots. DFA was performed using STATISTICA V.8.0 [47].

The Modified MixSIR Bayesian model was used to apportion the aeolian sediment source contributions. This model has been mainly used in sediment source tracing studies in fluvial systems [48–51], but more recently in aeolian and storm dust source tracing [19]. The model was run for 10^6 iterations with the nine different final composite fingerprints generated based on the different combinations of tracers. The maximum importance ratio was used to specify that the un-mixing model was effective in estimating the true posterior density distributions. Further details on this un-mixing model are provided in the aforementioned references.

To evaluate the MixSIAR predictions, known and modelled source contributions using each of the nine final composite fingerprints were compared on the basis of the root mean squared error (RMSE), mean absolute error (MAE), and Willmott's index of agreement (d) [23,51,52]. Comparison of known and modelled source proportions using this virtual mixture approach is now seen as an informative step in source fingerprinting procedures [15]. The model predictions of source proportions were evaluated using 7 sets of virtual sand dune mixtures for each composite signature for the three particle size fractions.

3. Results

3.1. Particle size fraction effects on elemental concentrations

The result of one-way ANOVA (Table 3) indicated that in the crop land source samples, concentrations of Al, Fe, Na, Si, and Ti were significantly affected by the absolute particle size fractions. Ti concentrations were higher in the < 125 µm fraction (finer size), whereas concentrations of Al, Fe, Na, and Si were higher in the medium (125–250 µm) size fraction of the crop land samples. In the case of the samples collected to represent both the western and south-eastern alluvial fan sources, concentrations of Fe, Na, and Si differed significantly by size fraction. Additionally, in both of these sources, Fe, Na, and Si concentrations were higher in the medium (125–250 µm fraction) size fraction. Critically, however, all tracers were present across all size fractions.

Table 3
The results of one-way ANOVA for the effect of particle size fractions on the elemental concentrations. Degree of freedom (df) = 2, SS, sum of square; MS, mean of square. *Critical p-value = 0.05.

Tracer	Aeolian sediment sources								
	Crop lands (total df = 41)			Western alluvial fans (total df = 32)			South-eastern alluvial fans (total df = 26)		
	SS	MS	F	SS	MS	F	SS	MS	F
Al	2.4	1.2	30.0*	1.9	0.9	1.9	4.0	2.0	0.7
Ca	8.2	4.1	2.6	31.3	15.6	1.3	42.7	21.4	0.1
Fe	142.0	71.0	1936.0*	170	85	45.6*	204.6	102.3	21.0*
K	0.68	0.34	2.4	0.9	0.5	1.6	0.6	0.3	1.5
Na	7.0	3.5	38.2*	2.5	1.2	52.6*	3.5	1.7	4.0*
Mg	0.77	0.38	0.79	0.4	0.2	1.0	0.02	0.009	0.018
Si	477.0	238.7	5.9*	76.5	38.2	26.8*	978.0	489.0	22.5*
Ti	0.001	0.0006	5.3*	0.001	0.0007	2.8	0.0003	0.0001	0.5

3.2. Final composite fingerprints for different particle size fractions

Final composite fingerprints for the < 125 µm fraction: The non-conservative tracers in this size fraction comprised Fe, K, Ti, MWPI, Si-Ti, ACN, AKN, Lc, and Rc. Using the KW-H test, 10 tracers were significant and thereby included in the second step for selecting composite fingerprints. The H-values for eight tracers (Na, Mg, Si, WIP, PI, RI, SA, Kr) in this size fraction exceeded 10 (Table 2).

1) Final composite fingerprint using only geochemical elements: Using the DFA, Mg, and Si were selected in the final composite signature (70.6% correct classification) for discriminating the sand dune sources (Table SI 1&2).

2) Final composite fingerprint using only weathering indices: Using DFA, PI, RI, and SOC were selected in the final signature (82.4% correct classification; Table SI 1&2).

3) Final composite fingerprint using a combination of geochemical elements and weathering indices: Using the DFA, Mg, PI, and RI were selected in the final composite signature (79.4% correct classification; Table SI 1&2).

Final composite fingerprints for the 125–250 µm fraction: In this fraction tracers including Fe, MWPI, PIA, and Lc were not conservative (Table 2). Using the KW-H test, 15 tracers were significant and used in DFA. The most significant tracers with high-H values were K, Na, Mg, Si, WIP, PI, CIW, SA, VR, Si-Ti, Kr, ACN, AKN, and ALK (Table 2).

1) Final composite fingerprint using only geochemical elements: Using the DFA, Na, and Mg, were selected in the final composite signature (76.5% correct classification) for discriminating the sand dune sources (Table SI 1&2).

2) Final composite fingerprint using only weathering indices: Using the DFA, PI, Si-Ti, CAN, and AKN were selected in the final composite signature (85.3% correct classification; Table SI 1&2).

3) Final composite fingerprint using combing the geochemical elements and weathering indices; Na, PI, VR, and Rc were selected in the final composite signature (94.1% classification; Table SI 1&2).

Final composite fingerprints for the 250–425 µm fraction: The results of conservation tests showed that in this fraction Ca, Si, CIA, MWPI, WIP, CIW, VR, Kr, Lc, and Rc were non-conservative tracers. Accordingly, these tracers were removed from the next step of the statistical procedure (Table 2). Using the KW-H test, 12 tracers were significant and applied in the DFA. The H-values showed that, in this fraction, five tracers (Fe, K, Na, PI, SOC) had high values exceeding 10 (Table 2).

1) Final composite fingerprint using only geochemical elements: Using the DFA, Fe, Na, and Mg were selected in the final composite signature (85.3% correct classification) for discriminating the sand dune sources (Table SI 1&2).

2) Final composite fingerprint using only weathering indices: Using the DFA, WIP, RI, AKN, ALK, and SOC were selected in the final signature (88.2% correct classification; Table SI 1&2).

3) Final composite fingerprint using combing the geochemical elements and weathering indices: Using the DFA, Fe, WIP, PI, RI, AKN, SOC were selected in the final signature (94.1% correct classification; Table SI 1&2).

The DFA scatter plots showing the source group discrimination visually for all nine final composite fingerprints are presented in Fig. 4.

Figure 5 shows biplots of the final tracers. These biplots demonstrated that the tracers selected in the final composite signatures had not been subjected to major transformation during redistribution from the

sampled sources to the target sand dune sampling locations.

3.2. Sand dune source contributions

For the < 125 μm fraction and using the geochemical elements composite signature, the mean relative contributions (5%-95% uncertainty ranges) from the crop lands, western alluvial fans, and south-eastern alluvial fans were estimated to be 1.5% (0.1–6.3%), 40.1% (28.6–49.1%), and 57.8% (48.9–69.3%), compared to 3.5% (0.3–10.8%), 32.1% (17.4–44.9%), and 63.6% (50.9–78.7%), using the weathering indices composite signature, or 1.6% (0.1–6.6%), 52.9% (42.4–65%), and 44.8% (32.2–55.8%), using the composite fingerprint combining geochemical elements and weathering indices (Fig. 6).

For the 125–250 μm fraction and using the geochemical elements composite signature, the mean relative contributions (5%-95% uncertainty ranges) from the crop lands, western alluvial fans, and south-eastern alluvial fans were estimated at 13.9% (3.7–24.7%), 76.4% (65-87.4%), and 8.6% (1.0-21.8%), compared to 11.4% (2.0-22.7%), 25.4% (11.0-38.7%), and 62.7% (51.0-75.8%), using the weathering indices composite signature, or 23.4% (10.4–34.8%), 0.7% (0.0-2.2%), and 75.9% (64.5–88.3%), using the signature combining geochemical elements and weathering indices (Fig. 6).

For the 250–425 μm fraction and using the geochemical elements composite signature, the relative contributions (5%-95% uncertainty ranges) from the crop lands, western alluvial fans, and south-eastern alluvial fans were predicted to be 5.6% (0.5–17.9%), 42.1% (26.1–52.6%), and 51.4% (43.8–61.7%), compared to 16.2% (3.6–29.9%), 41.8% (28.8–54.7%), and 41.4% (33.2–51.5%), using the weathering indices composite signature, or 15.5% (2.8–31.2%), 34.2% (19.2–46.5%), and 50.0% (43.9–57.5%), using the signature combining geochemical elements and weathering indices (Fig. 6).

4. Discussion

Using the < 125 μm fraction, the geochemical elements and weathering indices only composite signatures suggested that the south-eastern alluvial fan is the main source of the sand dunes (mean contributions of 57.8% and 63.6%, respectively), whereas the signature combining geochemical elements and weathering indices suggested that the western alluvial fan is the main source (52.9%) of the sampled sand dune sediment. Averaging the mean contributions predicted by using all three composite fingerprints, suggested that the south-eastern alluvial fan is the main source (55.4%) and the western alluvial fan the second most important (overall average 41.7%) source. The RMSE between the Modified MixSIR apportionment estimates for the contributions from crop lands, western alluvial fans, and south-eastern alluvial fans using the three final composite fingerprints were 1.6%, 14.8%, and 13.6%, respectively. The corresponding MAE was 1.3%, 13.9%, and 12.5%, whereas the d values were 0.2%, 0.33%, and 0.38% (Table 4).

For the 125–250 μm fraction, the geochemical elements composite signature indicated that the western alluvial fan is the main source (76.4%) of the sampled sand dune sediment, whereas both composite signatures comprising either weathering indices only or a combination of weathering indices and geochemical elements suggested that the south-eastern alluvial fan is the main source of the sampled

sand dune sediment (62.7%, and 75.9%, respectively). By averaging the contributions of all three composite signatures, the results showed that the south-eastern alluvial fan is the main source (49.1%) and the western alluvial fan (overall average 34.2%) the second most important source. The RMSE between the apportionment estimates for the contributions from crop lands, western alluvial fans, and south-eastern alluvial fans using the three final composite fingerprints was 9.0%, 54.6%, and 50.4% respectively. The corresponding MAE was 8.0%, 50.5%, and 44.9%. The corresponding d values were 0.42%, 0.33%, and 0.22% (Table 4).

In the 250–425 µm fraction, the geochemical elements and the composite signatures with either geochemical elements only or elemental geochemistry combined with weathering indices suggested that the south-eastern alluvial fans are the main source of the sampled sand dunes (51.4% and 50%, respectively). The weathering indices only composite signature suggested that the western alluvial fan is the main source of the sampled sand dunes (41.8%). By averaging the contributions of all three composite signatures, the results indicated that the south-eastern alluvial fan is the main source (47.6%) and the western alluvial fan (overall average 39.4%) the second most important source. The RMSE between the predicted contributions for for the crop lands, western alluvial fans, and south-eastern alluvial fans sources using the three final composite fingerprints was 8.4%, 6.3%, and 7.7%, respectively. The MAE was estimated to 7.1%, 5.3%, and 6.7%, whereas the d values were 0.04%, 0.47%, and 0.22% (Table 4).

Table 4
Comparison of the estimated relative contributions from the sand dune sources (1, crop lands; 2, western alluvial fans; 3, south-eastern alluvial fans) for different absolute particle size fractions using the three different composite signatures and the corresponding root mean squared error (RMSE), mean absolute error (MAE) and Willmott's index of agreement (d).

Composite fingerprints	Sand dune source proportions in the < 125 µm fraction			Sand dune source proportions in the 125–250 µm fraction			Sand dune source proportions in the 250–425 µm fraction		
	1	2	3	1	2	3	1	2	3
Geochemical elements only	1.5	40.1	57.8	13.9	76.4	8.6	5.6	42.1	51.4
Weathering indices only	3.5	32.1	63.6	11.4	25.4	62.7	16.2	41.8	41.4
Combination of geochemical elements and weathering indices	1.6	52.9	44.8	23.4	0.7	75.9	15.5	34.2	50
Overall average	2.2	41.7	55.4	16.2	34.2	49.1	12.4	39.4	47.6
Standard deviation	1.1	10.5	9.6	6.3	38.6	35.7	5.9	4.5	5.4
Differences between the estimated source proportions									
RMSE	1.6	14.8	13.6	9.0	54.6	50.4	8.4	6.3	7.7
MAE	1.3	13.9	12.5	8.0	50.5	44.9	7.1	5.3	6.7
d	0.20	0.33	0.38	0.42	0.33	0.22	0.04	0.47	0.22

All nine composite signatures for the different absolute particle size fractions suggested that the south-eastern alluvial fans are the dominant (overall average contribution 50.6%, SD 19.0%) source of the sand dunes samples. The western alluvial fans were estimated to be the second (overall average contribution 38.4%, SD 20.4%) most important source. The RMSE, MAE, and Willmott's index of agreement (d) estimates based on the nine composite tracers for the three particle size fractions ranged between 1.6% – 54.6% (with a mean value of 18.5%), 1.3% – 50.5% (with a mean value of 16.7%), and 0.04% – 0.5% (with a mean value of 0.3%), respectively (Table 4). Except in the 125–250 µm fraction for both the weathering indices only and a combination of the geochemical elements and weathering indices, the errors were acceptable for all other fractions. Similar findings have been reported by studies applying sediment source fingerprinting in both fluvial and aeolian systems [23,51,52].

In order to explore the efficiency of weathering indices there is a need to investigate these type of tracers during all fundamental steps of sediment source fingerprinting comprising conservation tests, discrimination of potential sources and source apportionment using an un-mixing model. Although conventional geochemical tracers are the most widely used in source fingerprinting studies [17], it remains

informative to test other kinds of tracers. Regardless of the absolute particle size fraction in question, 25% of the conventional geochemical tracers were non-conservative, while 33% of the weathering indices were non-conservative. After tracer selection using the conservation tests, 80% of the conventional geochemical tracers passed the KW-H test in < 125 µm fraction while 54.5% of weathering indices had significant value for this test in the same size fraction. In the 125–250 µm fraction, 57% of the conventional geochemical tracers passed the KW-H test while 78.6% of the weathering indices returned a significant value for this test. In the 250–425 µm fraction, 66% of the conventional geochemical tracers were significant using the KW-H test, while 70% of the weathering indices were significant. Overall, based on the statistical methods applied for tracer selection in this study, the weathering indices provided more statistically significant individual tracers for potential selection in the final composite signatures.

For the < 125 µm fraction, the discriminatory powers for conventional geochemical tracers only, weathering indices only, and a combination of geochemical tracers and weathering indices were 70.6%, 82.4%, and 79.4%, respectively. The corresponding efficiencies for the 125–250 µm fraction were 76.4%, 85.3%, and 94.1%; respectively. The discriminatory powers of the composite signatures comprising conventional geochemical tracers only, weathering indices only, and both combined for the 250–425 µm fraction were 85.3%, 88.2%, and 94.1%; respectively.The discriminatory power was therefore higher using the weathering indices across all size fractions. Except in the case of the finest fraction, source sample discrimination was highest when combining the conventional geochemical tracers and weathering indices. This underscores a key benefit of using weathering indices which provide a physico-chemical basis for helping to discriminate sediment sources [17]. Table 5 clearly shows that the estimated source contributions were sensitive to the kind of composite signature used, because all pairwise comparisons were significantly different ($p \leq 0.05$). Sediment sourcing studies should therefore apply more than one final composite signature to evaluate consistency in source predictions [15].

Table 5
Mann-Whitney U Test pairwise comparisons of the posterior probability density functions computed for the predicted contributions from the sand dune sources based on types of composite signatures in different particle size fractions.

Composite signature paired comparisons	Statistics	Sand dune sources		
		Crop lands	Western alluvial fans	South-eastern alluvial fans
< 125 µm fraction				
Geochemical elements vs. weathering indices	Adjusted Z	-36.0	48.5	-36.2
	p-level	< 0.0001	< 0.0001	< 0.0001
Geochemical elements vs. a combination of geochemical elements and weathering indices	Adjusted Z	-3.4	-63.1	62.8
	p-level	< 0.01	< 0.0001	< 0.0001
Weathering indices vs. a combination of geochemical elements and weathering indices	Adjusted Z	35.4	-90.0	87.7
	p-level	< 0.0001	< 0.0001	< 0.0001
125–250 µm fraction				
Geochemical elements vs. weathering indices	Adjusted Z	39.9	200.8	-200.0
	p-level	< 0.0001	< 0.0001	< 0.0001
Geochemical elements vs. a combination of geochemical elements and weathering indices	Adjusted Z	-49.0	76.6	-76.6
	p-level	< 0.0001	< 0.0001	< 0.0001
Weathering indices vs. a combination of geochemical elements and weathering indices	Adjusted Z	57.2	77.1	-60.8
	p-level	< 0.0001	< 0.0001	< 0.0001
250–425 µm fraction				
Geochemical elements vs. weathering indices	Adjusted Z	-107.8	-2.1	129.7

Composite signature paired comparisons	Statistics	Sand dune sources		
		Crop lands	Western alluvial fans	South-eastern alluvial fans
	p-level	< 0.0001	0.03	< 0.0001
Geochemical elements vs. a combination of geochemical elements and weathering indices	Adjusted Z	-96.5	76.9	25.3
	p-level	< 0.0001	< 0.0001	< 0.0001
Weathering indices vs. a combination of geochemical elements and weathering indices	Adjusted Z	7.0	97.5	-146.3
	p-level	< 0.01	< 0.0001	< 0.0001

For the < 125 μm fraction (Table 6), the RMSE, MAE, and d estimations based on the virtual mixture tests for the conventional geochemical tracers ranged between 2.3% − 26.7% (with an average value of 12.5%), 2.0% − 17.8% (with an average value of 10.9%), and 0.13–0.92 (with an average value of 0.61%), respectively. For the weathering indices, these values ranged between 2.6% − 30.5% (with an average value of 13%), 2.1% − 27.9% (with an average value of 11.6%), and 0.1–0.92 (with an average value of 0.56), respectively. For the final composite fingerprints combining conventional geochemical tracers and weathering indices, the corresponding values ranged between 5.5% − 21.5% (with an average value of 12.2%), 5.5% − 19.6% (with an average value of 10.8%), and 0.33–0.88 (with an average value of 0.72), respectively.

Table 6

Comparison of the predicted and known relative contributions from the sources to the virtual sand dune mixtures using the composite signatures and the corresponding root mean squared error (RMSE), mean absolute error (MAE), and Willmott's index of agreement (d) for the < 125 µm fraction.

Composite fingerprints	Known sand dune source proportions[1]			Predicted sand dune source proportions			RMSE	MAE	d
	1	2	3	1	2	3			
Conventional geochemical tracers	33.3	33.3	33.3	29.9	32.7	31.3	2.3	2.0	0.41
	50	25	25	31.7	29.8	32.7	11.8	10.3	0.13
	25	50	25	27.3	40.9	26	5.4	4.1	0.91
	25	25	50	31.2	25.7	38.5	7.6	6.1	0.80
	75	10	15	35.5	25.2	33.5	26.7	24.4	0.37
	15	75	10	22.8	54.4	17.1	13.4	11.8	0.92
	10	15	75	30.4	19.1	45.9	20.7	17.9	0.73
Weathering indices	33.3	33.3	33.3	30.1	32.2	30.3	2.6	2.4	0.39
	50	25	25	27.6	29.4	36.1	14.7	12.6	0.06
	25	50	25	21.6	40.6	31.7	6.9	6.5	0.87
	25	25	50	23.7	24.4	45.6	2.7	2.1	0.99
	75	10	15	29.7	31.3	32.2	30.6	27.9	0.00
	15	75	10	23.4	44.6	25.8	20.4	18.2	0.73
	10	15	75	19.5	19.8	54.8	13.2	11.5	0.92
Combination of conventional geochemical tracers and weathering indices	33.3	33.3	33.3	39.3	28.4	27.8	5.5	5.5	0.33
	50	25	25	37.1	25	33.4	8.9	7.1	0.71
	25	50	25	28.7	39.3	27.7	6.7	5.7	0.85
	25	25	50	32.1	22	41.7	6.5	6.1	0.88
	75	10	15	43.3	21.9	30.3	21.5	19.6	0.68
	15	75	10	27.7	48.1	19.3	18.0	16.3	0.81
	10	15	75	29.1	17.1	49.8	18.3	15.5	0.81

[1]sand dune sources comprising: 1, crop lands; 2, western alluvial fans; and 3, south-eastern alluvial fans.

For the 125–250 μm fraction (Table 7), the estimates of RMSE, MAE, and d for the virtual mixture tests for the conventional geochemical tracers ranged between 3.2% – 24.5% (with an average value of 11.8%), 3.2% – 22.3% (with an average value of 10.5%), and 0.45–0.93 (with an average value of 0.68), respectively. For the composite fingerprints comprising weathering index tracers only, the values ranged between 4.5% – 19.8% (with an average value of 11.0%), 3.6% – 18.2% (with an average value of 9.8%), and 0.29–0.94 (with an average value of 0.72), respectively. For the final composite fingerprints combining both conventional geochemical tracers and weathering indices, the values ranged between 1.7% – 54.5% (with an average value of 14.6%), 1.5% – 39.7% (with an average value of 11.3%), and 0.01–1.0 (with an average value of 0.65), respectively.

Table 7

Comparison of the predicted and known relative contributions from the sources to the virtual sand dune mixtures using the different composite signatures and the corresponding root mean squared error (RMSE), mean absolute error (MAE), and Willmott's index of agreement (d) for the 125–250 µm fraction.

Composite fingerprints	Known sand dune source proportions[1]			Predicted sand dune source proportions			RMSE	MAE	d
	1	2	3	1	2	3			
Conventional geochemical tracers	33.3	33.3	33.3	29.6	35.6	29.8	3.2	3.2	0.45
	50	25	25	36	29.4	29.9	8.9	7.8	0.64
	25	50	25	24	42.4	28.9	5.0	4.2	0.93
	25	25	50	27.1	34.3	33.9	10.8	9.2	0.45
	75	10	15	50	18.7	26.2	16.6	15.0	0.85
	15	75	10	16.4	54.3	24.1	14.5	12.1	0.90
	10	15	75	24.4	31.6	39.2	24.3	22.3	0.52
Weathering indices	33.3	33.3	33.3	37.2	33.3	26.1	4.7	3.7	0.29
	50	25	25	42.8	28.2	25.5	4.6	3.6	0.94
	25	50	25	29.7	39.3	27.9	7.0	6.1	0.83
	25	25	50	30.3	31	35.4	9.6	8.6	0.53
	75	10	15	55.5	20.5	20.5	13.2	11.8	0.92
	15	75	10	24.8	48	24	18.4	16.9	0.79
	10	15	75	22.8	27.5	45.7	19.8	18.2	0.75
Combination of conventional geochemical tracers and weathering indices	33.3	33.3	33.3	38.1	33.8	27.9	4.2	3.6	0.01
	50	25	25	47.8	24.9	27.1	1.8	1.5	0.99
	25	50	25	27.4	49.7	22.6	2.0	1.7	0.99
	25	25	50	40.5	24.6	34.9	12.5	10.3	0.46
	75	10	15	61.8	103	27.9	54.7	39.7	0.44
	15	75	10	12.7	74.3	12.3	1.9	1.8	1.00
	10	15	75	41.2	14.1	44.5	25.2	20.9	0.63

[1]sand dune sources comprising: 1, crop lands; 2, western alluvial fans; and 3, south-eastern alluvial fans.

Lastly, for the 250–425 μm fraction (Table 8), the estimates of RMSE, MAE, and d using the conventional geochemical tracers only ranged between 3.2% − 18.9% (with an average value of 9.8%), 2.5% − 16.1% (with an average value of 8.5%), and 0.34–0.98 (with an average value of 0.77), respectively. Using the weathering indices only, the corresponding values ranged between 4.2% − 27.6% (with an average value of 16.7%), 3.5% − 23.2% (with an average value of 14.6%), and 0.11–0.98 (with an average value of 0.52), respectively. Using the final composite fingerprints combining conventional geochemical tracers and weathering indices, the values ranged between 4.9% − 32.1% (with an average value of 16.8%), 4.6% − 26.9% (with an average value of 14.9%), and 0.22–0.99 (with an average value of 0.56), respectively.

Table 8

Comparison of the predicted and known relative contributions from the sources to the virtual sand dune mixtures using the different composite signatures and the corresponding root mean squared error (RMSE), mean absolute error (MAE), and Willmott's index of agreement (d) for the 250–425 µm fraction.

Composite fingerprints	Known sand dune source proportions[1]			Predicted sand dune source proportions			RMSE	MAE	d
	1	2	3	1	2	3			
Conventional geochemical tracers	33.3	33.3	33.3	27.9	38.4	29.5	4.8	4.8	0.34
	50	25	25	35.7	34.7	25.2	10.0	8.1	0.61
	25	50	25	26.8	44.8	24.3	3.2	2.6	0.98
	25	25	50	24.7	30.8	39.7	6.8	5.5	0.85
	75	10	15	48.6	29.3	17.5	18.9	16.1	0.79
	15	75	10	24.3	60	11.6	10.2	8.6	0.96
	10	15	75	19	23.9	52	15.2	13.6	0.88
Weathering indices	33.3	33.3	33.3	53.6	24.4	19	15.2	14.5	0.11
	50	25	25	53.5	24.4	18.6	4.2	3.5	0.98
	25	50	25	49.7	30	17	18.9	17.6	0.29
	25	25	50	42.6	23.7	29.7	15.5	13.1	0.24
	75	10	15	60.8	21.6	14.7	10.6	8.7	0.95
	15	75	10	45.5	38.2	12.3	27.6	23.2	0.55
	10	15	75	34.5	21	40	24.9	21.8	0.53
Combination of conventional geochemical tracers and weathering indices	33.3	33.3	33.3	52.6	20.8	24.4	14.2	13.6	0.08
	50	25	25	60.3	19.3	18.7	7.7	7.4	0.94
	25	50	25	56.2	24.3	17.8	23.7	21.4	0.22
	25	25	50	44	18.6	34.8	14.5	13.5	0.48
	75	10	15	70	16.4	12.5	4.9	4.6	0.99
	15	75	10	54.9	36.4	7.8	32.1	26.9	0.48
	10	15	75	31.9	17.2	47.6	20.3	17.2	0.75

[1]sand dune sources comprising: 1, crop lands; 2, western alluvial fans; and 3, south-eastern alluvial fans.

Overall, for the finer fraction, the RMSE, MAE, and d values from the virtual mixture tests using the different composite signatures showed that the signatures combining the geochemical elements and weathering indices returned the greatest accuracy. For the medium particle size fraction, the composite fingerprints based on the weathering indices alone returned the best accuracy. For the coarsest fraction, the conventional geochemical composite fingerprints returned the most accurate predictions of source contributions.

There are inevitably some limitations associated with the different steps of this source fingerprinting study. Determining the sand dune sources map is very difficult and complex because the main erosive agent for this study is wind erosion. In this study we only selected the sources that are surrounded by mountains to decrease the potential impacts of regional winds on patterns of sand mobilisation and redistribution. Accordingly, our source sampling only needed to consider the prevailing local wind directions based on the wind rose. Sampling design and sample collection are also important stages of source fingerprinting. In the case of environments dominated by wind erosion processes, the terrain is frequently flat meaning that the conventional approach to targeting source sampling using visual appraisals of connectivity pathways along steeper terrain is not useful. In addition, seasonal changes in prevailing wind directions need to be given due consideration. The temporal and spatial scales of sampling for aeolian environments are therefore likely to differ from those associated with applications of source fingerprinting in environmental settings dominated by hydro-fluvial processes. Depending on the tracers being used, it could be informative to assess the presence of seasonal variations in source tracer properties. Equally, in some settings, both fluvial and aeolian processes will be interacting in the erosion and redistribution of sediments, including, for instance, in the case of abandoned stream channels. Here, it will be necessary to design sampling strategies encompassing the sources impacted by water and wind agents.

5. Conclusions

Our results demonstrate that the use the weathering indices in addition to conventional elemental geochemistry can be useful for investigations into sand dune sediment provenance. Assembling reliable information on the provenance of aeolian sediment deposits supports the targeting of source-control mitigation measures instead of sand dune stabilization interventions including chemical mulching which can suffer from unintended consequences. Future research should expand assessment of the application of weathering indices in combination with more conventional fingerprint properties to additional aeolian and storm sand systems since there is an ongoing need to assist management of the aeolian sediment problem globally.

Declarations

Acknowledgements:

Grant number 600.3294 from the research council of Shahid Beheshti University has supported this research. Mojtaba Dolatkordestani as a postdoctoral researcher has been funded to work at Shahid Beheshti University by the Iran National Science Foundation (INSF) (grant number 98012293). ALC was supported by strategic funding from UKRI-BBSRC (UK Research and Innovation - Biotechnology and Biological Sciences Research Council (grant BBS/E/C/000I0330; Soil to Nutrition project 3).

References

1. Chepil, W. Dynamics of wind erosion: I. Nature of movement of soil by wind. *Soil Science* **60**, 305-320 (1945).
2. Pi, H., Webb, N. P., Huggins, D. R. & Sharratt, B. Critical standing crop residue amounts for wind erosion control in the inland Pacific Northwest, USA. *Catena* **195**, 104742 (2020).
3. Fryrear, D. W. Soil cover and wind erosion. *Transactions of the ASAE* **28**, 781-0784 (1985).
4. Zobeck, T. M. Soil properties affecting wind erosion. *Journal of Soil and Water Conservation* **46**, 112-118 (1991).
5. Al-Hemoud, A. *et al.* Sand and dust storm trajectories from Iraq Mesopotamian flood plain to Kuwait. *Science of The Total Environment* **710**, 136291 (2020).
6. Al-Hemoud, A. *et al.* Economic Impact and Risk Assessment of Sand and Dust Storms (SDS) on the Oil and Gas Industry in Kuwait. *Sustainability* **11**, 200 (2019).
7. Refahi, H. *Wind erosion and its control*. 320 (in Persian) (Tehran University, Iran, 2004).
8. Zoraghi, G., Goraji, K. S., Noura, M., Rashki, A. & Bumby, A. An assessment of the ability of a novel mulch to stabilise sand dunes in the Sistan region of Iran. *International Journal of Environmental Studies*, 1-14 (2021).
9. Mombeni, M., Asgari, H. R., Behbahani, A. M., Zare, S. & Yousefi, H. Effect of bagasse lignocellulose microfibers on sand stabilization: A laboratory study. *Aeolian Research* **49**, 100654 (2021).
10. Rezaie, S. Comparison between polylatice polymer and petroleum mulch on seed germination and plant establishment in sand dune fixation. *Iranian Journal of Range and Desert Research* **16**, 124-136 (in Persian) (2009).
11. Lancaster, N. & Ollier, C. Sources of sand for the Namib sand sea. *Zeitschrift für Geomorphologie* **45**, 73-83 (1983).
12. Merriam, R. Source of Sand Dunes of Southeastern California and Northwestern Sonora, Mexico. *GSA Bulletin* **80**, 531-534, doi:10.1130/0016-7606(1969)80[531:sosdos]2.0.co;2 (1969).
13. Muhs, D. R. & Budahn, J. R. New geochemical evidence for the origin of North America's largest dune field, the Nebraska Sand Hills, central Great Plains, USA. *Geomorphology* **332**, 188-212 (2019).
14. Muhs, D. R., Bush, C. A., Cowherd, S. D. & Mahan, S. in *Desert Aeolian Processes* (ed V.P. Tchakerian) 37-74 (Springer, 1995).
15. Collins, A. *et al.* Sediment source fingerprinting as an aid to catchment management: a review of the current state of knowledge and a methodological decision-tree for end-users. *Journal of*

Environmental Management **194**, 86-108 (2017).

16. Owens, P. *et al.* Fingerprinting and tracing the sources of soils and sediments: Earth and ocean science, geoarchaeological, forensic, and human health applications. *Earth-Science Reviews* **162**, 1-23 (2016).
17. Collins, A. L. *et al.* Sediment source fingerprinting: benchmarking recent outputs, remaining challenges and emerging themes. *Journal of Soils and Sediments*, doi:10.1007/s11368-020-02755-4 (2020).
18. Gholami, H., Kordestani, M. D., Li, J., Telfer, M. W. & Fathabadi, A. Diverse sources of aeolian sediment revealed in an arid landscape in southeastern Iran using a modified Bayesian un-mixing model. *Aeolian Research* **41**, 100547 (2019).
19. Nosrati, K. *et al.* Storm dust source fingerprinting for different particle size fractions using colour and magnetic susceptibility and a Bayesian un-mixing model. *Environmental Science and Pollution Research*, 1-17 (2020).
20. Liu, B., Niu, Q., Qu, J. & Zu, R. Quantifying the provenance of aeolian sediments using multiple composite fingerprints. *Aeolian Research* **22**, 117-122 (2016).
21. Mohammadi Raigani, Z., Nosrati, K. & Collins, A. L. Fingerprinting sub-basin spatial sediment sources in a large Iranian catchment under dry-land cultivation and rangeland farming: Combining geochemical tracers and weathering indices. *Journal of Hydrology: Regional Studies* **24**, 100613, doi:https://doi.org/10.1016/j.ejrh.2019.100613 (2019).
22. Motha, J., Wallbrink, P., Hairsine, P. & Grayson, R. Determining the sources of suspended sediment in a forested catchment in southeastern Australia. *Water resources research* **39** (2003).
23. Nosrati, K., Fathi, Z. & Collins, A. L. Fingerprinting sub-basin spatial suspended sediment sources by combining geochemical tracers and weathering indices. *Environmental Science and Pollution Research* **26**, 28401-28414, doi:10.1007/s11356-019-06024-x (2019).
24. Pye, K. & Tsoar, H. in *Aeolian Sand and Sand Dunes* Ch. three, 51-97 (Springer, 2009).
25. Lancaster, N. *Geomorphology of Desert Dunes*. (Psychology Press, 1995).
26. Guo, Y. *et al.* Revisiting the effects of hydrodynamic sorting and sedimentary recycling on chemical weathering indices. *Geochimica et Cosmochimica Acta* **227**, 48-63, doi:https://doi.org/10.1016/j.gca.2018.02.015 (2018).
27. Shao, J., Yang, S. & Li, C. Chemical indices (CIA and WIP) as proxies for integrated chemical weathering in China: inferences from analysis of fluvial sediments. *Sedimentary Geology* **265**, 110-120 (2012).
28. Négrel, P., Sadeghi, M., Ladenberger, A., Reimann, C. & Birke, M. Geochemical fingerprinting and source discrimination of agricultural soils at continental scale. *Chemical Geology* **396**, 1-15 (2015).
29. Buggle, B., Glaser, B., Hambach, U., Gerasimenko, N. & Marković, S. An evaluation of geochemical weathering indices in loess–paleosol studies. *Quaternary International* **240**, 12-21 (2011).

30. Li, C. & Yang, S. Is chemical index of alteration (CIA) a reliable proxy for chemical weathering in global drainage basins? *American Journal of Science* **310**, 111-127 (2010).
31. Ohta, T. & Arai, H. Statistical empirical index of chemical weathering in igneous rocks: A new tool for evaluating the degree of weathering. *Chemical Geology* **240**, 280-297 (2007).
32. Nesbitt, H. W. & Young, G. M. Early Proterozoic climates and plate motions inferred from major element chemistry of lutites. *Nature* **299**, 715-717, doi:10.1038/299715a0 (1982).
33. Vogel, D. Precambrian weathering in acid metavolcanic rocks from the Superior Province, Villebon Township, South-central Quebec. *Canadian Journal of Earth Sciences* **12**, 2080-2085 (1975).
34. Parker, A. in *Geological Magazine* Vol. 107 501-504 (1970).
35. Guo, Y., Yang, S., Li, C., Bi, L. & Zhao, Y. Sediment recycling and indication of weathering proxies. *Acta Geochimica* **36**, 498-501 (2017).
36. Price, J. R. & Velbel, M. A. Chemical weathering indices applied to weathering profiles developed on heterogeneous felsic metamorphic parent rocks. *Chemical Geology* **202**, 397-416, doi:https://doi.org/10.1016/j.chemgeo.2002.11.001 (2003).
37. Ruxton, B. P. Measures of the degree of chemical weathering of rocks. *The Journal of Geology* **76**, 518-527 (1968).
38. Harnois, L. The CIW index: A new chemical index of weathering. *Sedimentary Geology* **55**, 319-322, doi:https://doi.org/10.1016/0037-0738(88)90137-6 (1988).
39. Fedo, C., Wayne Nesbitt, H. & Young, G. Unraveling the effects of potassium metasomatism in sedimentary rocks and paleosols, with implications for paleoweathering conditions and provenance. *Geology* **23**, 921-924, doi:10.1130/0091-7613(1995)023<0921:UTEOPM>2.3.CO;2 (1995).
40. Garzanti, E. From static to dynamic provenance analysis—Sedimentary petrology upgraded. *Sedimentary Geology* **336**, 3-13 (2016).
41. Guan, P., Ng, C., Sun, M. & Tang, W. Weathering indices for rhyolitic tuff and granite in Hong Kong. *Engineering Geology* **59**, 147-159 (2001).
42. Jayawardena, U. d. S. & Izawa, E. Application of present indices of chemical weathering for Precambrian metamorphic rocks in Sri Lanka. *Bulletin of the International Association of Engineering Geology-Bulletin de l'Association Internationale de Géologie de l'Ingénieur* **49**, 55-61 (1994).
43. Moignien, R. *Review of Research on Laterites*. (United Nations Educational. Scientific and Cultural Organization (UNESCO), 1966).
44. Harnois, L. & Moore, J. M. Geochemistry and origin of the Ore Chimney Formation, a transported paleoregolith in the Grenville Province of southeastern Ontario, Canada. *Chemical Geology* **69**, 267-289 (1988).
45. Ng, C., Guan, P. & Shang, Y. Weathering mechanisms and indices of the igneous rocks of Hong Kong. *Quarterly Journal of Engineering Geology and Hydrogeology* **34**, 133-151 (2001).
46. Irfan, T. Mineralogy, fabric properties and classification of weathered granites in Hong Kong. *Quarterly Journal of Engineering Geology and Hydrogeology* **29**, 5-35 (1996).

47. STATISTICA: [data analysis software system], Version 8.0 for Windows update. StatSoft, Inc. v. 8.0 for Windows update (2008).
48. Nosrati, K., Govers, G., Semmens, B. X. & Ward, E. J. A mixing model to incorporate uncertainty in sediment fingerprinting. *Geoderma* **217**, 173-180 (2014).
49. Nosrati, K. Ascribing soil erosion of hillslope components to river sediment yield. *Journal of Environmental Management* **194**, 63-72, doi:https://doi.org/10.1016/j.jenvman.2016.10.011 (2017).
50. Nosrati, K., Collins, A. L. & Madankan, M. Fingerprinting sub-basin spatial sediment sources using different multivariate statistical techniques and the Modified MixSIR model. *Catena* **164**, 32-43 (2018).
51. Nosrati, K. & Collins, A. L. Fingerprinting the contribution of quarrying to fine-grained bed sediment in a mountainous catchment, Iran. *River Research and Applications* **35**, 290-300, doi:10.1002/rra.3408 (2019).
52. Nosrati, K. & Collins, A. L. Investigating the importance of recreational roads as a sediment source in a mountainous catchment using a fingerprinting procedure with different multivariate statistical techniques and a Bayesian un-mixing model. *Journal of Hydrology* **569**, 506-518, doi:https://doi.org/10.1016/j.jhydrol.2018.12.019 (2019).

Table

Due to technical limitations, table 1 docx is only available as a download in the Supplemental Files section.

Figures

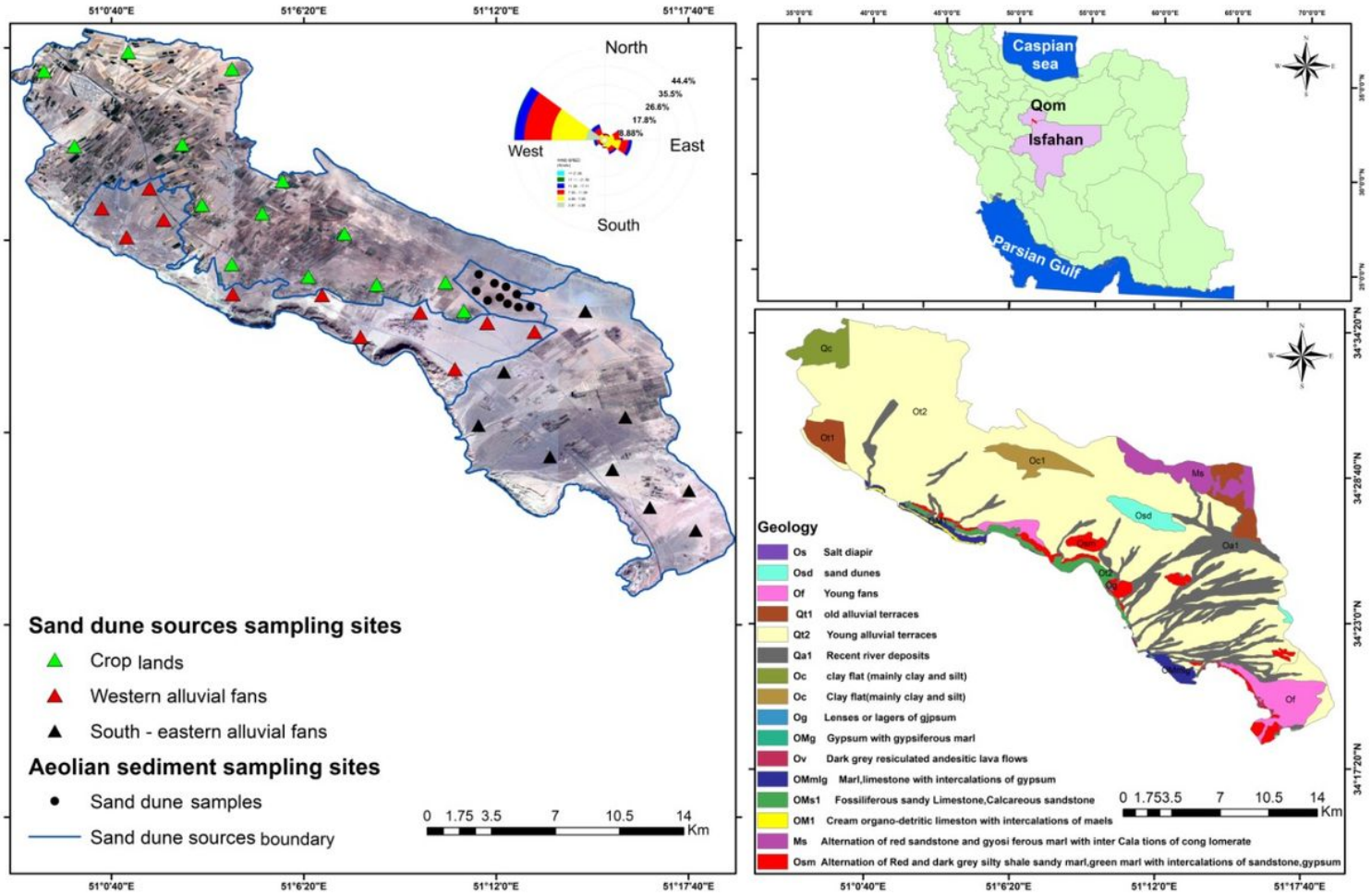

Figure 1

Map of the study area in central Iran, showing the predominant wind directions and the source and target aeolian sediment sampling locations. Note: The designations employed and the presentation of the material on this map do not imply the expression of any opinion whatsoever on the part of Research Square concerning the legal status of any country, territory, city or area or of its authorities, or concerning the delimitation of its frontiers or boundaries. This map has been provided by the authors.

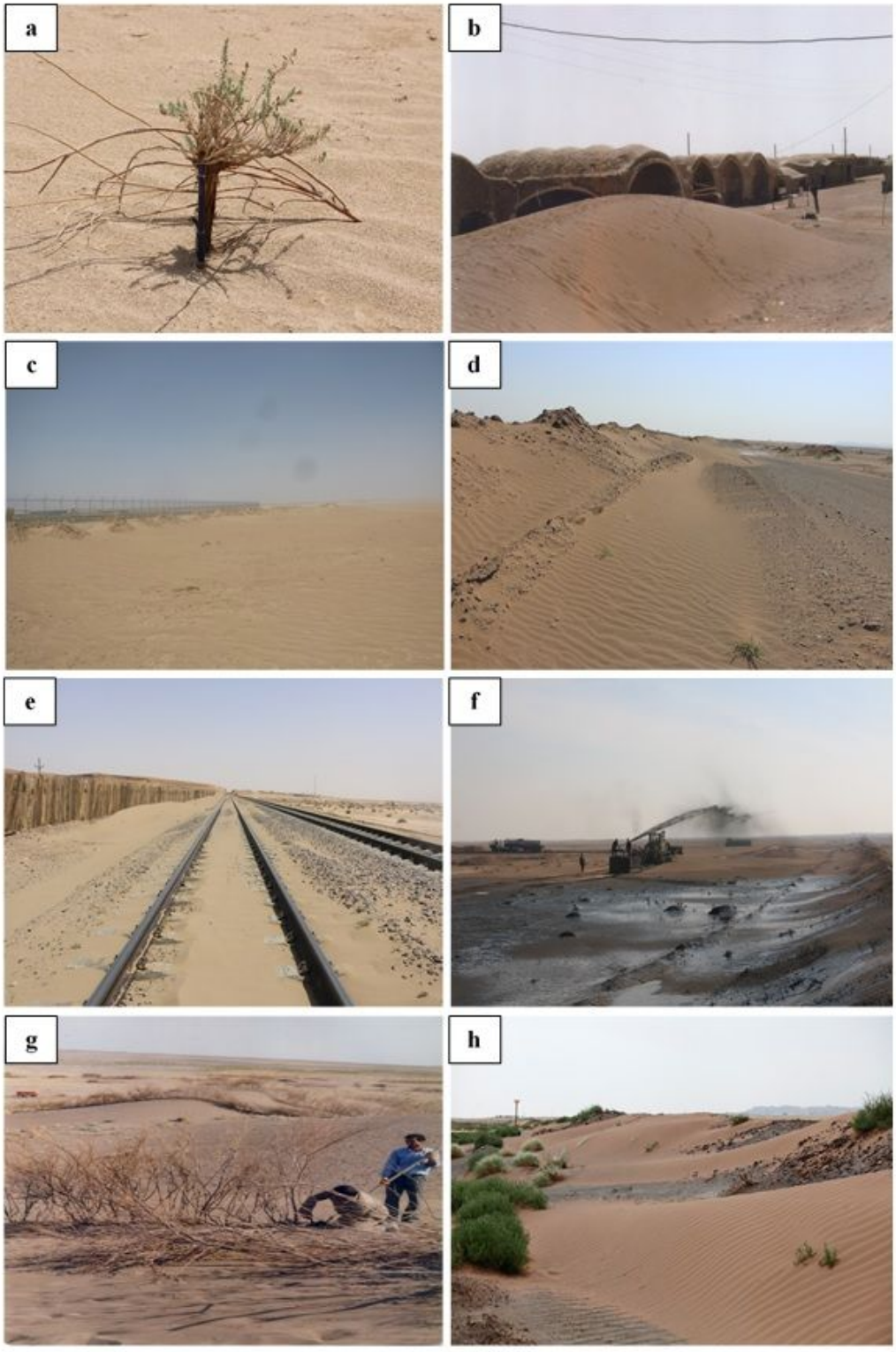

Figure 2

Photos showing severe wind erosion (a); sand dunes threatening residential areas (village) (b), gas supply installation (c), emergency road (d), and railway (as well inefficient windbreak) (e); soil protection against wind erosion provided by petroleum and tar derived mulching (f), a natural windbreak (g) and; destroyed mulch (h).

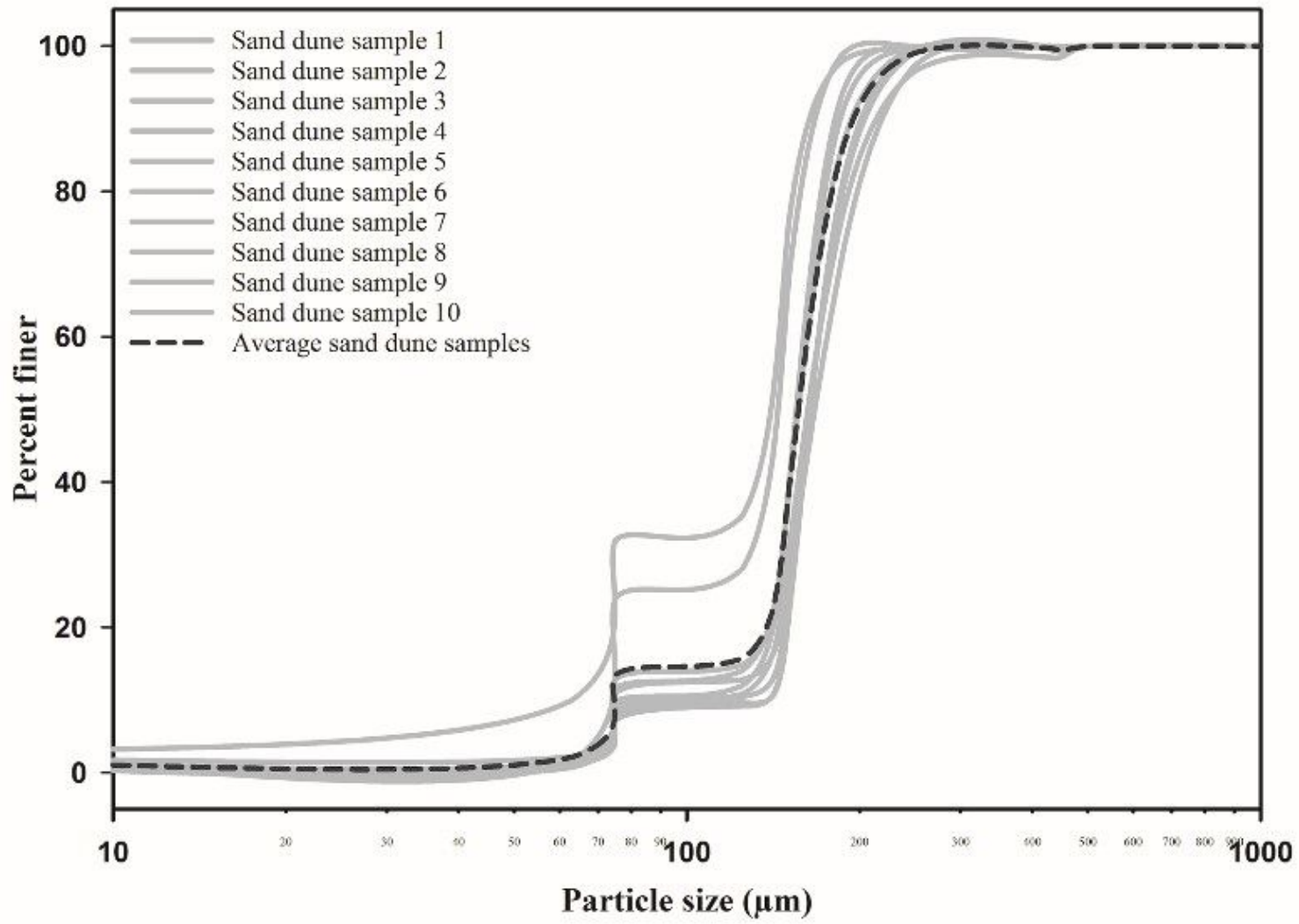

Figure 3

The absolute particle size distributions of the target aeolian sediment (i.e., sand dune) samples.

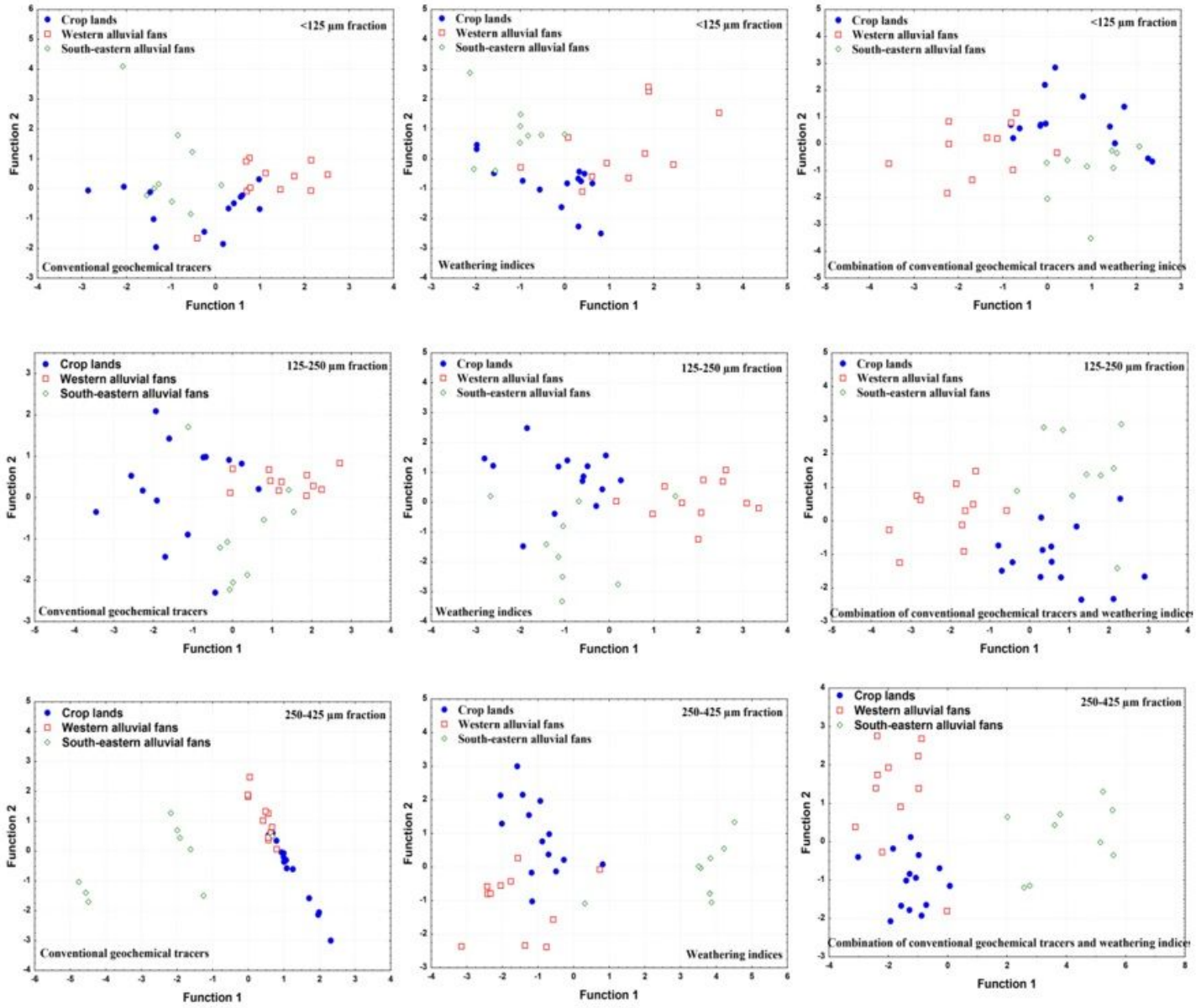

Figure 4

Scatterplots of the first and second discriminant functions calculated using DFA for the different absolute particle size fractions.

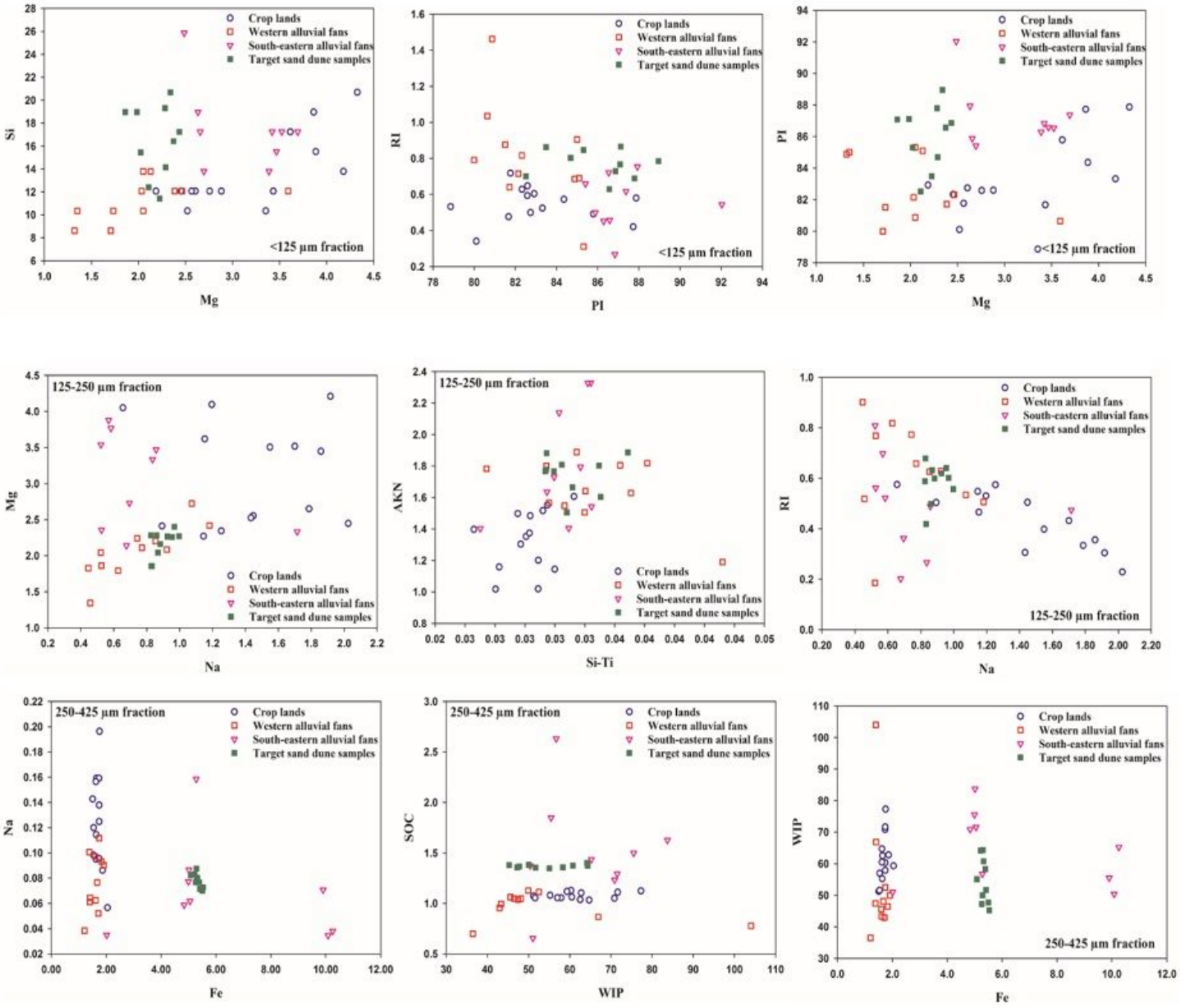

Figure 5

Biplots of all pairings for some tracers selected in the final composite signatures for discriminating and apportioning the sand dune source contributions.

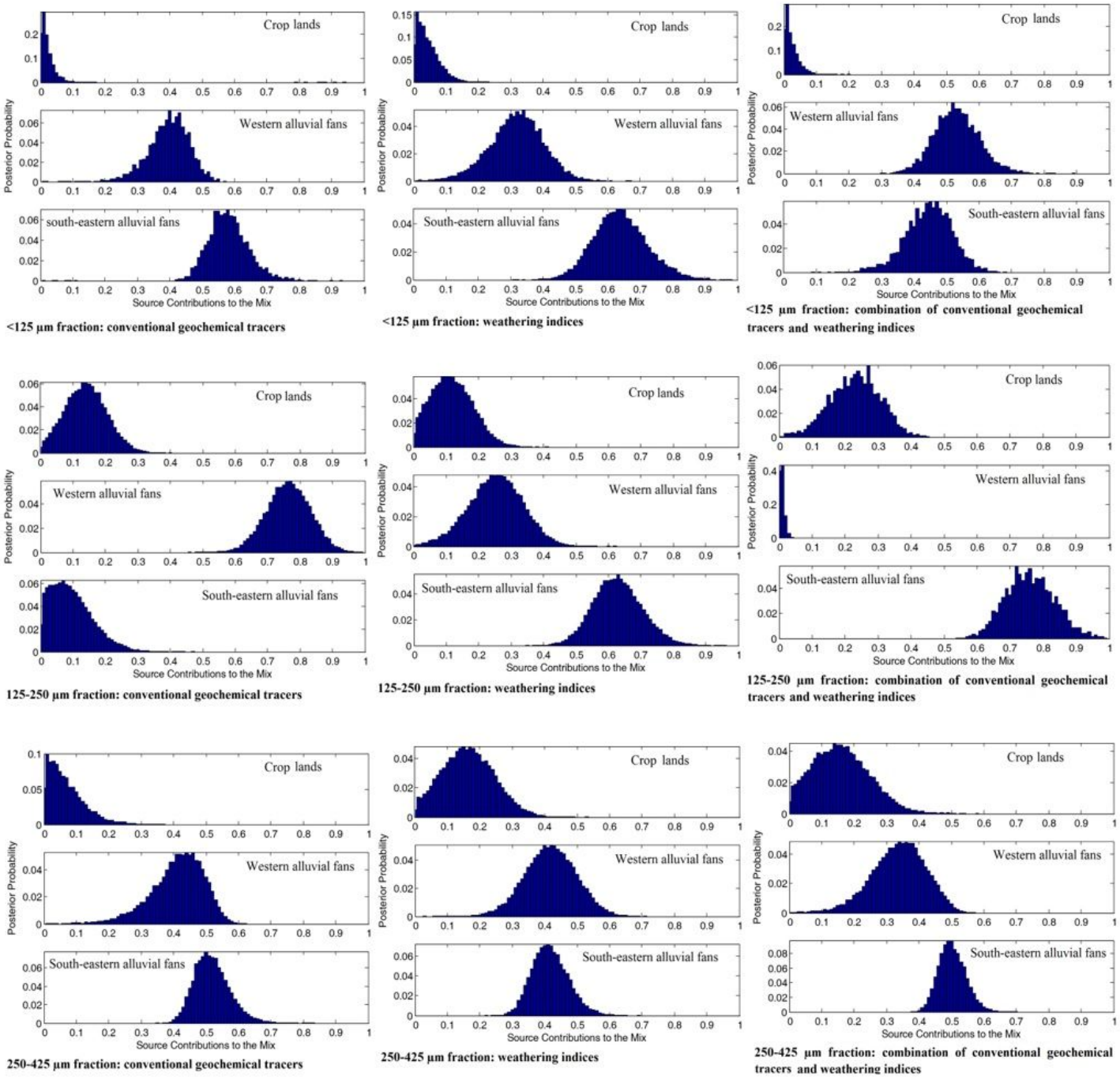

Figure 6

Modified MixSIR estimated sand dune source contributions using composite signatures for the different absolute particle size fractions.

Supplementary Files

This is a list of supplementary files associated with this preprint. Click to download.

- SupplamentaryInformation.docx

- Table1.docx